NEUROSCIENCE

Descending pathways mediate adaptive optimized coding of natural stimuli in weakly electric fish

Chengjie G. Huang*, Michael G. Metzen†, Maurice J. Chacron†‡

Biological systems must be flexible to environmental changes to survive. This is exemplified by the fact that sensory systems continuously adapt to changes in the environment to optimize coding and behavioral responses. However, the nature of the underlying mechanisms remains poorly understood in general. Here, we investigated the mechanisms mediating adaptive optimized coding of naturalistic stimuli with varying statistics depending on the animal's velocity during movement. We found that central neurons adapted their responses to stimuli with different power spectral densities such as to optimally encode them, thereby ensuring that behavioral responses are, in turn, better matched to the new stimulus statistics. Sensory adaptation further required descending inputs from the forebrain as well as the raphe nuclei. Our findings thus reveal a previously unknown functional role for descending pathways in mediating adaptive optimized coding of natural stimuli that is likely generally applicable across sensory systems and species.

INTRODUCTION

Growing evidence suggests that sensory systems optimally encode natural stimuli by incorporating statistical information about environmental signals (*1*–*3*). However, because natural stimulus statistics vary with time, sensory neurons must adjust their responses (i.e., adapt) in order for their encoding efficiency to remain optimal (*4*). While sensory adaptation has been observed ubiquitously across systems and species (*5*), the nature of the underlying mechanisms remains poorly understood to this day. Moreover, how adaptive optimized coding by sensory neurons affects behavioral performance has not been systematically investigated to date.

The electrosensory system of wave-type gymnotiform weakly electric fish is an attractive model system for understanding the neural basis of behavior (*6*). These fish generate a quasi-sinusoidal signal of individual frequency called the electric organ discharge (EOD) around their bodies and rely on perturbations of this signal to acquire information about their environment. In particular, when two fish are in proximity to each other (<2 m) (*7*, *8*), their EODs interfere with one another, and the interaction between the two frequencies generates a sinusoidal amplitude modulation (AM) of the EOD whose contrast (i.e., envelope) strongly depends on the distance and orientation between both fish (*9*). Recent studies have focused on understanding the statistics of these signals in the environment and have found that they display scale invariance as the spectral power decays as a power law with an exponent of −0.8 with increasing temporal frequency (*10*). EOD perturbations including envelopes are sensed by an array of electroreceptor afferents (EAs), which project to pyramidal cells (PCells) within the electrosensory lateral line lobe (ELL). PCells are the sole output neurons of the ELL and project to higher brain structures, thereby giving rise to behavior (*6*). The response properties of ELL PCells to envelope stimuli have been extensively studied [see (*11*) for review]. In particular, it was found that ELL PCell response properties were matched to natural envelope statistics such as to optimally encode them, which, in turn, ensures that behavioral sensitivity is matched to stimulus statistics (*12*). The response properties of ELL PCells to envelopes are strongly dependent on descending input from higher brain centers (*13*). However, these previous studies for the most part did not consider changes in envelope stimulus statistics. While we have demonstrated that ELL PCells display adaptation in response to artificial (i.e., step) changes in envelope (*14*), changes that occur in more natural settings have not been considered to date. We thus investigated whether ELL PCells can alter their response properties such as to optimally encode envelope stimuli with different statistics that better reflect changes in the natural environment and the consequences of such sensory adaptation on behavior.

Department of Physiology, McGill University, 3655 Sir William Osler, Montreal, QC, Canada.
*Present address: Ear Institute, University College London, London, UK.
†These authors contributed equally to this work.
‡Corresponding author. Email: maurice.chacron@mcgill.ca

RESULTS

We recorded neural and behavioral responses in awake behaving weakly electric fish to envelope stimuli. Briefly, the animal was placed in a tank while head-tail electrodes recorded behavioral responses consisting of changes in the animal's EOD frequency and stimuli were delivered via two electrodes located on each side (Fig. 1, top). This setup allows the simultaneous recording of neural and behavioral responses. We have previously shown that the response properties of ELL PCells are matched to natural stimulus statistics such as to allow optimal encoding via temporal whitening (*12*). Such optimized coding by sensory neurons in turn ensures that behavioral sensitivity is matched to natural stimulus statistics such that both decay similarly with increasing frequency. Such matching makes intuitive sense as behavioral sensitivity is highest for frequencies that are most represented in natural electrosensory stimuli (*11*, *12*). Here, we investigated whether neural and behavioral responses were adaptable to stimuli with different statistics and investigated the nature of the underlying mechanisms. ELL PCells receive feedforward sensory input from EAs and project to higher brain centers including the midbrain torus semicircularis (TS) and the telencephalon (Tel) (Fig. 1, bottom) that generate behavioral responses. As mentioned above, ELL PCells also receive large amounts of feedback from Tel and TS as well as neuromodulatory inputs from the raphe nuclei (Fig. 1, bottom).

Central electrosensory neurons adapt their properties such as to optimally encode stimuli with different statistics

We investigated how neural and behavioral responses adapt to stimuli whose statistics differ from that found under natural conditions. We

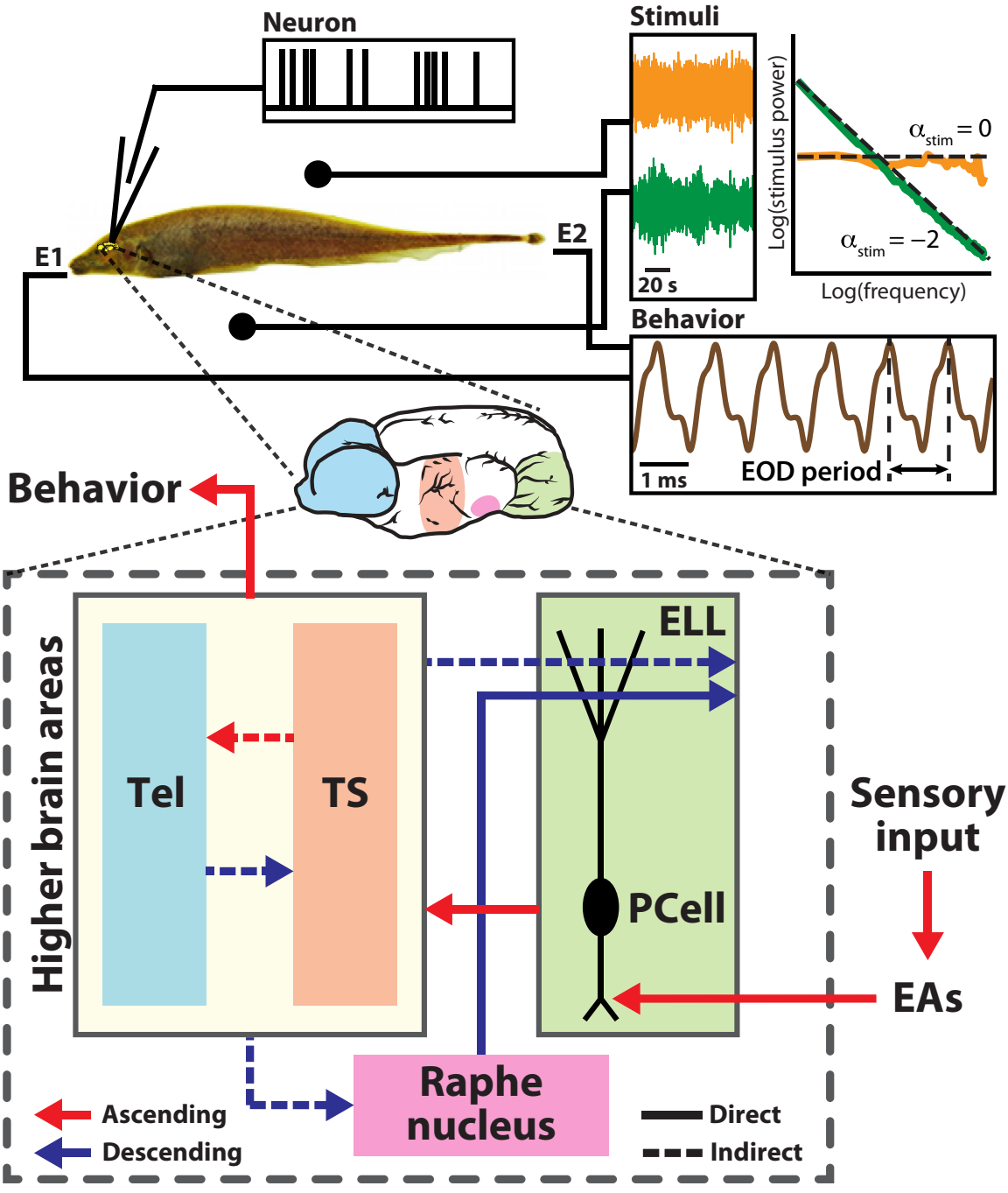

Fig. 1. Experimental setup and relevant circuitry. Top: The fish is placed in an experimental tank. Behavioral responses consisting of changes in the EOD are recorded via two electrodes (E1 and E2) placed at the head and tail of the fish, respectively. Neural recordings were obtained by placing electrodes in the brain. Stimuli were delivered via two other electrodes (dark solid circles) placed on either side of the fish. We used stimuli whose power spectral density either decayed strongly with increasing frequency (i.e., characterized by a power law exponent of −2, green) or was constant (i.e., characterized by a power law exponent of 0, orange). Bottom: Simplified circuit diagram in which sensory input is transduced and sent via EAs to PCells within the ELL. PCells project to higher brain areas that mediate behavioral responses including the midbrain TS and indirectly to Tel. PCells also receive large amounts of descending input (i.e., feedback) indirectly from Tel via TS as well as neuromodulatory feedback from the raphe nuclei. Photo credit: Maurice Chacron at McGill University.

thus used two adaptation stimuli that have approximately the same overall power in the frequency range 0 to 1 Hz but have different power-frequency relationships: One whose power is independent of frequency (i.e., characterized by a power law exponent of 0) and another whose power decays sharply with increasing frequency (i.e., characterized by a power law exponent of −2) (Fig. 1, top; see Materials and Methods). These exponents were chosen such as to strongly differ from the exponent found under natural conditions (i.e., −0.8) and thus maximize the probability of eliciting sensory adaptation. Our protocol consisted of presenting either stimulus and comparing ELL PCell

responses in the early and late phases of the stimulus presentation (see Materials and Methods). Overall, if ELL PCells display sensory adaptation, we would expect that their responses do not match the statistics of either stimulus and, thus, not optimally encode them initially (Figs. 2A and 3A, middle panels, solid black lines), as the power law exponents differ from those found under natural conditions (Figs. 2A and 3A, left, compare dashed and solid black lines). Hence, the response power spectra should initially not be independent of frequency (i.e., not temporally whitened; Figs. 2A and 3A, middle, solid black lines). However, if adaptation occurs such as to more optimally encode the stimulus over time, then we would expect a gradual shift in ELL PCell response properties to better match the adapting stimulus' statistics. This would then result in the response power spectral density becoming more independent of frequency (i.e., temporally whitened; Figs. 2A and 3A, middle panels, solid green and orange lines).

Our results show that ELL PCell responses gradually adapted when a stimulus characterized with a power law exponent of −2 was presented (Fig. 2B). The response power initially strongly depended on frequency (Fig. 2B, left) but gradually became more independent of frequency (Fig. 2B, right), which is a signature of optimized coding. We quantified our results using a whiteness index measure that is equal to unity if the power spectral density is independent of frequency and is less otherwise (see Materials and Methods). Our results show that the whiteness index gradually increased as a function of time (Fig. 2C, left). Overall,

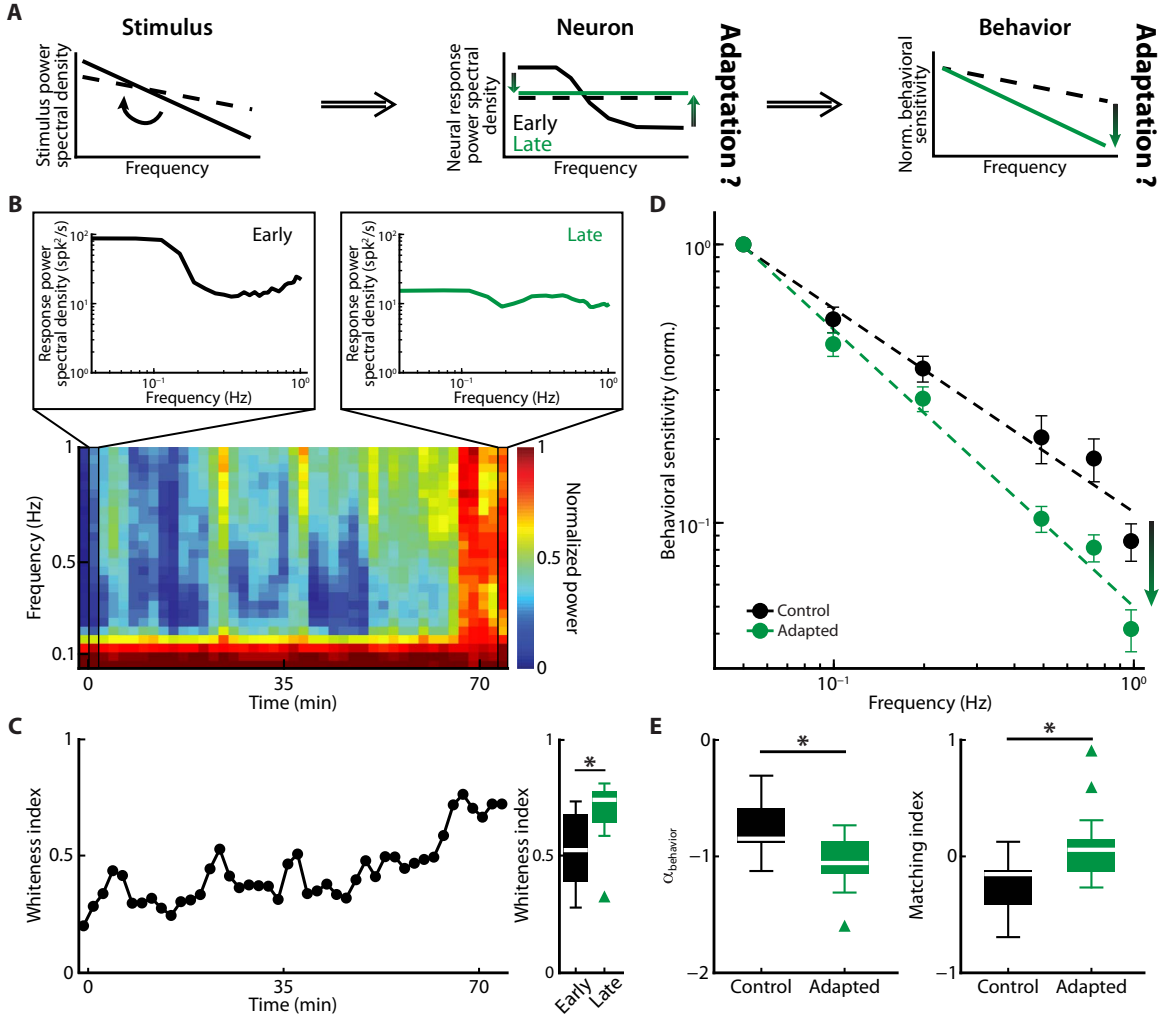

Fig. 2. ELL PCells adapt their responses such as to optimally encode stimuli characterized by a power law exponent of −2. (**A**) Schematic showing the adaptation stimulus power spectral density (left, solid black) together with that of natural stimuli (left, dashed black). Previous studies have shown that PCells optimally encode natural stimuli. Hence, their response power spectral density to these is constant (middle, dashed black). We predict that the PCell response power spectral density to the adaptation stimulus will initially not be independent of frequency (e.g., low pass; middle, solid black) but will gradually become more independent of frequency (middle, green) via adaption. Behavioral sensitivity is initially matched to natural stimulus statistics (right, dashed black). We predict that adaptation at the behavioral level will lead to changes in behavioral sensitivity such as to better match the statistics of the adaptation stimulus (right, solid green). (**B**) Spectrogram (i.e., running time power spectral density) of the response of an example PCell to the adaptation stimulus. The upper left and right insets show the response power spectral densities as a function of frequency for this cell early (left) and late (right) during stimulus presentation. (**C**) Left: Whiteness index as a function of time for this same PCell. Right: Whisker-box plots showing the population-averaged whiteness index values early and late during stimulus presentation. (**D**) Population-averaged behavioral sensitivity as a function of frequency before (black) and after (green) stimulus presentation. (**E**) Left: Population-averaged behavioral exponents before (black) and after (green) stimulus presentation. Right: Population-averaged matching index values before (black) and after (green) stimulus presentation. *$P = 0.05$ (Wilcoxon signed rank test).

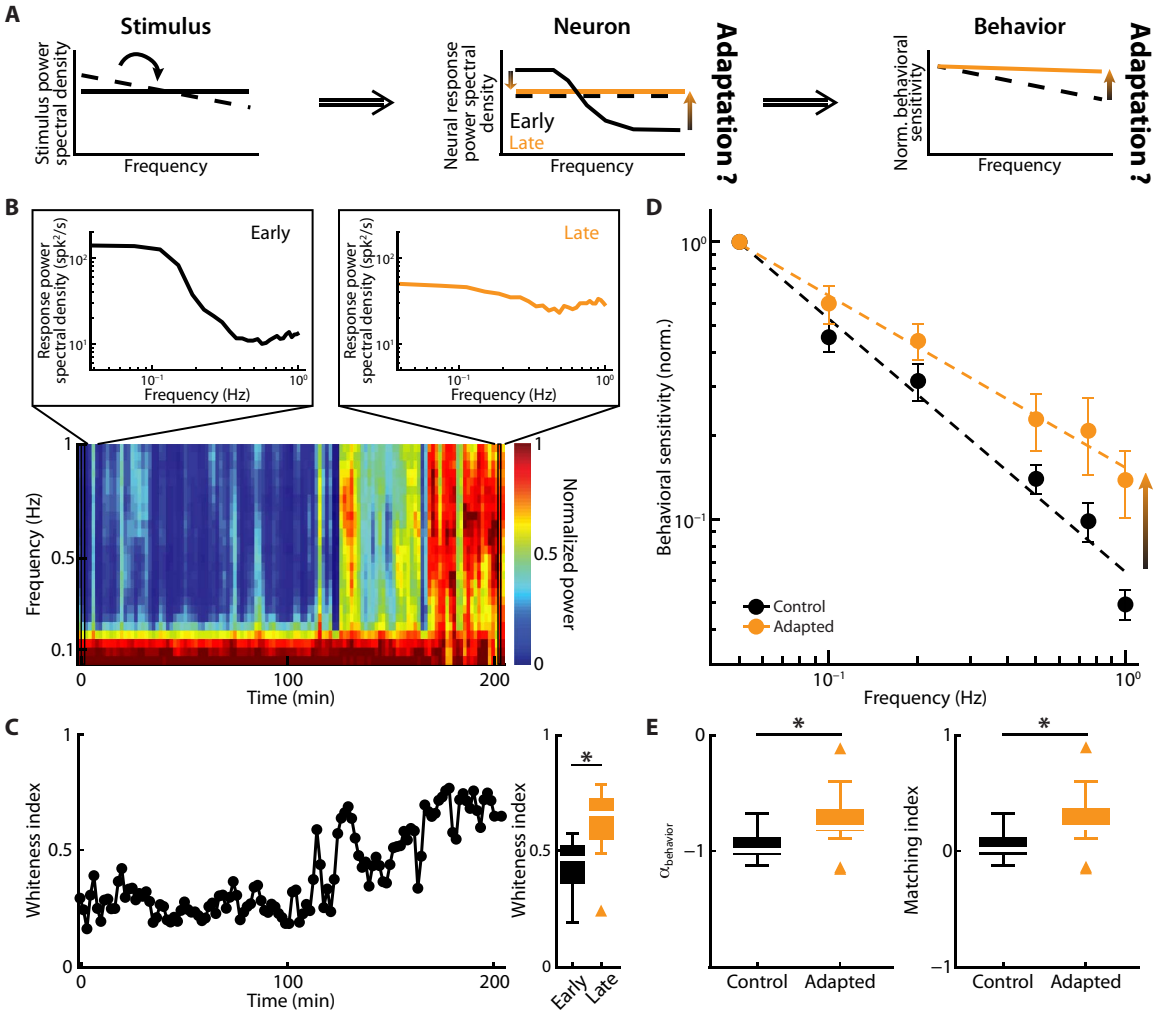

Fig. 3. ELL PCells adapt their responses such as to optimally encode stimuli characterized by a power law exponent of 0. (**A**) Same as Fig. 2A but for an adaptation stimulus with exponent 0. (**B**) Spectrogram (i.e., running time power spectral density) of the response of an example PCell to the adaptation stimulus. The upper left and right insets show the response power spectral densities as a function of frequency for this cell early (left) and late (right) during stimulus presentation. (**C**) Left: Whiteness index as a function of time for this same PCell. Right: Whisker-box plots showing the population-averaged whiteness index values early and late during stimulus presentation. (**D**) Population-averaged behavioral sensitivity as a function of frequency before (black) and after (orange) stimulus presentation. (**E**) Left: Population-averaged behavioral exponents before (black) and after (orange) stimulus presentation. Right: Population-averaged matching index values before (black) and after (orange) stimulus presentation. *P = 0.05 (Wilcoxon signed rank test).

qualitatively similar results were obtained when instead presenting a stimulus characterized with a power law exponent of 0 (Fig. 3, B and C). The response power spectral density gradually became more independent of frequency (i.e., more temporally whitened; Fig. 3B) as quantified by whiteness index values that increased as a function of time (Fig. 3C). Across our dataset, we found that the whiteness index late during stimulus presentation was significantly higher than that computed immediately after stimulus onset (Fig. 2C, right: $\alpha_{stim} = -2$, compare black and green, $n = 16$, $P = 1.2 \times 10^{-4}$; Fig. 3C, right: $\alpha_{stim} = 0$, compare black and orange, $n = 15$, $P = 9.8 \times 10^{-4}$, Wilcoxon signed rank tests). We note that changes in the response power spectral density were not due to changes in firing rate (FR), coefficient of variation (CV), or burst fraction (BF). This is because these did not significantly change between immediately after stimulus onset and late during stimulus presentation (fig. S1A; $\alpha_{stim} = -2$: FR, $P = 0.12$; CV, $P = 0.43$; BF, $P = 0.10$; fig. S2A; $\alpha_{stim} = 0$: FR, $P = 1.00$; CV, $P = 0.58$; BF, $P = 0.37$, Wilcoxon signed rank tests). Moreover, interspike interval (ISI) distributions early and late during stimulus presentation were not significantly different from one another (fig. S1, B and C, $\alpha_{stim} = -2$, $P = 0.78$; fig. S2, B and C, $\alpha_{stim} = 0$, $P = 0.48$; Kolmogorov-Smirnov tests). Thus, our results demonstrate that the response properties of ELL PCells actively change such as to more optimally encode stimuli that are characterized by different power law exponents.

We next investigated how the response properties of ELL PCells changed to optimally encode sensory input in an adaptive manner. Earlier studies have suggested that optimized coding can be achieved when neural sensitivity (i.e., tuning) increases to compensate for the decaying stimulus power, such that the stimulus is filtered by the neural transfer function, thereby removing redundancy (*12*, *15*). This approach, however, fails to take into account neural variability (see Materials and Methods and Eq. 2), which can have significant impact on filtering (*16*). Rather, theory suggests that optimized coding is achieved by

ensuring that both neural sensitivity (i.e., tuning) and variability are matched to natural stimulus statistics, as recently demonstrated experimentally in the vestibular system (*3*, *17*). This latter case corresponds more to "information filtering" in which the signal-to-noise ratio is considered. Hence, we hypothesized that changes in ELL PCell response properties must involve changes in their tuning as well as variability to optimally encode stimuli in an adaptive manner. To test this, we measured ELL PCell tuning properties as well as their variability before and after presentation of the adaptation stimulus. Our results show that changes in ELL PCell response properties cannot be accounted for by changes in tuning alone, irrespective of whether tuning was measured in response to sinusoidal stimulation (fig. S3) or to the adaptation stimulus itself (fig. S4). Rather, our results show that adaptive optimized coding can be explained by changes in tuning and variability, as considering changes in both is necessary to correctly predict experimental data (fig. S5).

Adaptive optimized coding by central electrosensory neurons ensures matching between behavioral sensitivity and stimulus statistics

Do changes in ELL PCell response properties influence behavior? To investigate this important question, we took advantage of the fact that weakly electric fish give robust behavioral responses to sinusoidal sensory input in that their EOD frequency tracks the time course of the sensory input in a one-to-one fashion. Previous studies have shown that the sensitivity of this behavioral response is matched to natural stimulus statistics (*10*, *12*). Hence, we predict that, if adaptive optimized coding by ELL PCells is behaviorally relevant, behavioral responses should better match the adapting stimulus' statistics late in adaptation (Figs. 2A and 3A, right). To test this hypothesis, we compared the animal's behavioral sensitivity using sinusoidal stimuli at different frequencies before and after adaptation (see Materials and Methods). We found that, over time, behavioral sensitivity shifted (fig. S6, A and B), such that the best-fit power law exponent was closer to that of the adaptation stimulus (Fig. 2, D and E, left; $\alpha_{stim} = -2$; $\alpha_{control} = -0.79 \pm 0.05$, black; $\alpha_{adapted} = -1.08 \pm 0.07$, green, $P = 1.3 \times 10^{-3}$, Wilcoxon signed rank test; Fig. 3, D and E, left: $\alpha_{stim} = 0$; $\alpha_{control} = -0.94 \pm 0.03$, black; $\alpha_{adapted} = -0.72 \pm 0.07$, orange, $P = 4.3 \times 10^{-3}$, Wilcoxon signed rank test). As a result, there was a better match late in adaptation between the best-fit power law exponents of the adaptation stimulus power spectral density and behavioral sensitivity, as quantified by significant increases in the matching index (Fig. 2E, right; $\alpha_{stim} = -2$; control = -0.21 ± 0.05, black; adapted = 0.07 ± 0.06, green, $P = 1.3 \times 10^{-3}$; Fig. 3E, right; $\alpha_{stim} = 0$; control = 0.06 ± 0.13, black; adapted = 0.28 ± 0.07, orange, $P = 4.3 \times 10^{-3}$; Wilcoxon signed rank tests; see Materials and Methods). We note that this match was not perfect as the best-fit behavioral exponent did not reach that of the adaptation stimulus in each case. This is discussed below.

Stimulus statistics encountered in the environment depend on the animal's level of activity

We next asked whether the power spectral densities of stimuli experienced by weakly electric fish change in a manner mimicking the adaptation stimuli used in this study (i.e., are characterized by different power law exponents). To do so, we recorded the interactions between pairs of fish in a seminaturalistic setting where one animal is freely moving while another is restrained in a tube (Fig. 4A). We subsequently extracted movement trajectories from video recordings as well as the simultaneous electrosensory stimuli recorded by a dipole placed adjacent to the fish in the tube (Fig. 4A, $N = 4$ pairs, 90 min each).

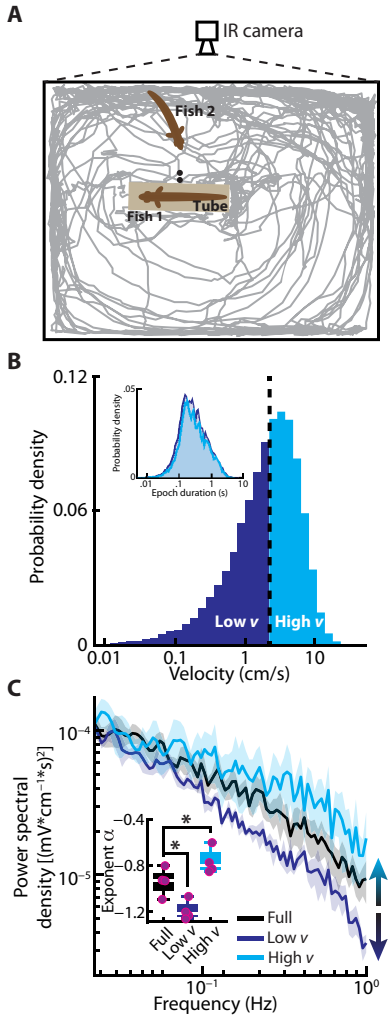

Fig. 4. Stimulus statistics depend on the level of activity in weakly electric fish. (**A**) Schematic of the tank setup with an infrared (IR) camera recording of a stationary fish inside a tube (fish 1) and another freely moving fish (fish 2) with trajectories in gray. A small dipole located close to the tube recorded the stimuli experienced by fish 1 (black circles). (**B**) Probability density of the velocities of fish 2 for all recordings ($N = 4$) with division of low (dark blue) versus high (light blue) velocities (see Materials and Methods). The dashed line indicates the median velocity. The inset shows the probability densities of epoch duration during which the velocity was low (dark blue) and high (light blue) velocities. These overlapped and were thus not significantly different from one another. (**C**) Power spectral densities of the stimuli as a function of stimulus frequency for the full (black), low (dark blue), and high (light blue) velocity stimuli. Inset: Whisker-box plots showing the best-fit power-law exponents for the envelopes of the corresponding stimuli. *$P = 0.05$ (Wilcoxon signed rank test).

We then segregated the obtained signals into periods when the fish's velocity was lower and higher (see Materials and Methods). When considering the entire dataset, we found that the stimulus power decayed with a power law exponent close to −0.8 ($\alpha_{full} = -0.93 \pm 0.04$), consistent with previous studies (*10*). We then considered epochs when the longitudinal velocity was either below (i.e., "low velocity") or above (i.e., "high velocity") its median value (Fig. 4B). The distributions of duration of epochs during which the animal's velocity was low or high were not significantly different from one another (Fig. 4B, inset; $P = 0.07$, Kolmogorov-Smirnov test). Overall, we found that, for periods

of low velocity, the stimulus power spectral density decayed more sharply with increasing frequency as quantified by a significantly lower power law exponent ($\alpha_{low} = -1.19 \pm 0.04$; $P = 2.6 \times 10^{-2}$, t test; Fig. 4C, dark blue). In contrast, for periods of high velocity, the stimulus power spectral density decayed less sharply with increasing frequency as quantified by a significantly higher power law exponent ($\alpha_{high} = -0.76 \pm 0.06$; $P = 9.6 \times 10^{-3}$, t test; Fig. 4C, light blue). We note that analysis of surrogate data where epochs were chosen randomly showed no significant differences between the exponents (fig. S7A). Qualitatively similar results were seen when changing the threshold over a wide range of values (fig. S7B). These results show that stimulus statistics depend on velocity. We hypothesize that weakly electric fish will experience stimuli characterized by different power law exponents in their natural environment as detailed below.

Feedback from the Tel is necessary for sensory and behavioral adaptation

What is the nature of the mechanisms underlying sensory adaptation by ELL PCells? Previous studies have shown that sensory input is conveyed via midbrain structures to Tel, which in turn projects back to ELL (Fig. 1, bottom). We hypothesize that sensory adaptation is caused by a descending signal that originates from Tel. To test this hypothesis, we first lesioned Tel prior to presenting the adaptation stimulus (Fig. 5A). Overall, we found that the neural response power spectral density strongly depended on frequency and did not change as a function of time after lesioning Tel (Fig. 5B, compare left and right), as quantified by the whiteness index measure that was more or less constant as a function of time (Fig. 5C, left). As a result, the population-averaged whiteness index values early and late in adaptation were not significantly different from one another (Fig. 5C, right; $n = 8$, $P = 0.31$, Wilcoxon signed rank test). We further note that the whiteness index values early in adaptation after lesioning Tel were not significantly different from those obtained under control conditions ($P = 0.95$, Wilcoxon rank sum). FR, CV, BF, and ISI distributions were not significantly altered during stimulus presentation after lesioning Tel (fig. S8). We further note that lesioning forebrain did not significantly alter response properties initially [fig. S8, A (compare gray and black box plots), figs. S8, B, C]. Thus, our results indicate that lesioning Tel did not affect neural responses overall but strongly impaired sensory adaptation. The lack of change in neural response power was furthermore correctly predicted by our theory (fig. S8D). Lesioning Tel also strongly impaired behavioral adaptation as behavioral sensitivity no longer significantly changed during stimulus presentation (Fig. 5, D and E, left, and fig. S8E). The population-averaged behavioral exponents before and after presenting the adaptation stimulus were not significantly different from one another (Fig. 5E, left; $n = 9$; $\alpha_{control(lesion)} = -0.97 \pm 0.07$, $\alpha_{adapted(lesion)} = -0.90 \pm 0.04$; $n = 8$, $P = 0.20$, Wilcoxon signed rank test). We further note that the behavioral exponent after lesion was not significantly different than that obtained before lesioning Tel (Fig. 5E, left; $P = 0.46$, Wilcoxon signed rank test). As a result, there were no significant changes in matching index values overall [Fig. 5E, right; control, 0.02 ± 0.08; $control_{lesion}$, -0.11 ± 0.08; $adapted_{lesion}$, -0.12 ± 0.04; $n = 8$, $P_{control/control(lesion)} = 0.46$, $P_{control(lesion)/adapted(lesion)} = 0.20$, Wilcoxon signed rank tests].

Sensory and behavioral adaptation require serotonergic neuromodulatory feedback

From our above findings showing that lesioning the forebrain prevents sensory adaptation, we next wanted to investigate the feedback pathways originating from higher brain areas and how these interact with ELL PCells. We therefore tested whether serotonergic feedback from the raphe nuclei was necessary for sensory adaptation in contrast to the direct or indirect pathways from TS to ELL. To do so, we injected the 5-HT2 receptor antagonist ketanserin (KET) while recording from ELL PCells and/or measuring behavioral responses before presenting the adaptation stimulus (Fig. 6A). Overall, results qualitatively similar to those observed after lesioning the forebrain were observed in that neural responses no longer changed in response to the adaptation stimulus (Fig. 6B) as quantified by the whiteness index (Fig. 6C). The population-averaged whiteness index values early and late in adaptation were not significantly different from one another after KET application ($n = 8$, $P = 0.38$, Wilcoxon signed rank). We note that KET application did not alter neural responses, as the whiteness index values early in adaptation were not significantly different than those found under control conditions (i.e., no KET application; $P = 0.16$, Wilcoxon signed rank test). Furthermore, FR, CV, BF, and ISI distributions were not significantly different between early and late during stimulus presentation after injecting KET (fig. S9). We further note that KET injection did not significantly alter these response properties [fig. S9, A (compare gray and black box plots), figs. S9, B, C]. The lack of change in neural response power was furthermore correctly predicted by our theory (fig. S9D). Moreover, behavioral responses did not change after presenting the adaptation stimulus (Fig. 6, D and E, left, and fig. S9E), as the behavioral exponents were not significantly different from one another [Fig. 6E, left; $\alpha_{control} = -1.07 \pm 0.11$, gray; $\alpha_{control\ (KET)} = -1.11 \pm 0.13$, black; $\alpha_{adapted\ (KET)} = -1.13 \pm 0.09$, green; $n = 8$, $P_{control/control(KET)} = 0.74$, $P_{control(KET)/adapted(KET)} = 0.84$, Wilcoxon signed rank tests]. As a result, there were no significant changes in matching index values overall (Fig. 6E, right; control, 0.07 ± 0.11; $control_{KET}$, 0.11 ± 0.13; $adapted_{KET}$, 0.13 ± 0.10; $n = 8$, $P_{control/control(KET)} = 0.74$, $P_{control(KET)/adapted(KET)} = 0.84$, Wilcoxon signed rank tests). Our results thus reveal a previous unknown function for serotonergic pathways in that they are required for sensory adaptation.

DISCUSSION

Summary of results

Here, we investigated whether ELL PCells can adapt their response properties to optimally encode stimuli with different statistics, the consequences of adaptation on behavior, as well as the nature of the underlying mechanisms. Our results show that, when stimuli characterized with different power law exponents were presented, the power spectral densities of ELL PCell responses changed progressively such as to become more independent of frequency, a signature of optimal coding. Changes in ELL PCell response properties were due to changes in both tuning and variability and led to changes in behavioral sensitivity to better match the adapting stimulus' statistics. We also measured electrosensory stimulus statistics and found that stimuli associated with different longitudinal velocities were characterized by different power law exponents. We then investigated the nature of the mechanisms that underlie sensory adaptation by ELL PCells. We found that lesioning the forebrain did not alter ELL neural or behavioral responses but prevented adaptation. Further, we found that injecting the serotonergic receptor antagonist KET also prevented adaptation and did not alter ELL neural or behavioral responses.

Natural electrosensory stimulus statistics change over time

Previous studies have investigated the statistics of the sensory input experienced by weakly electric fish (*9*, *10*) but have not considered

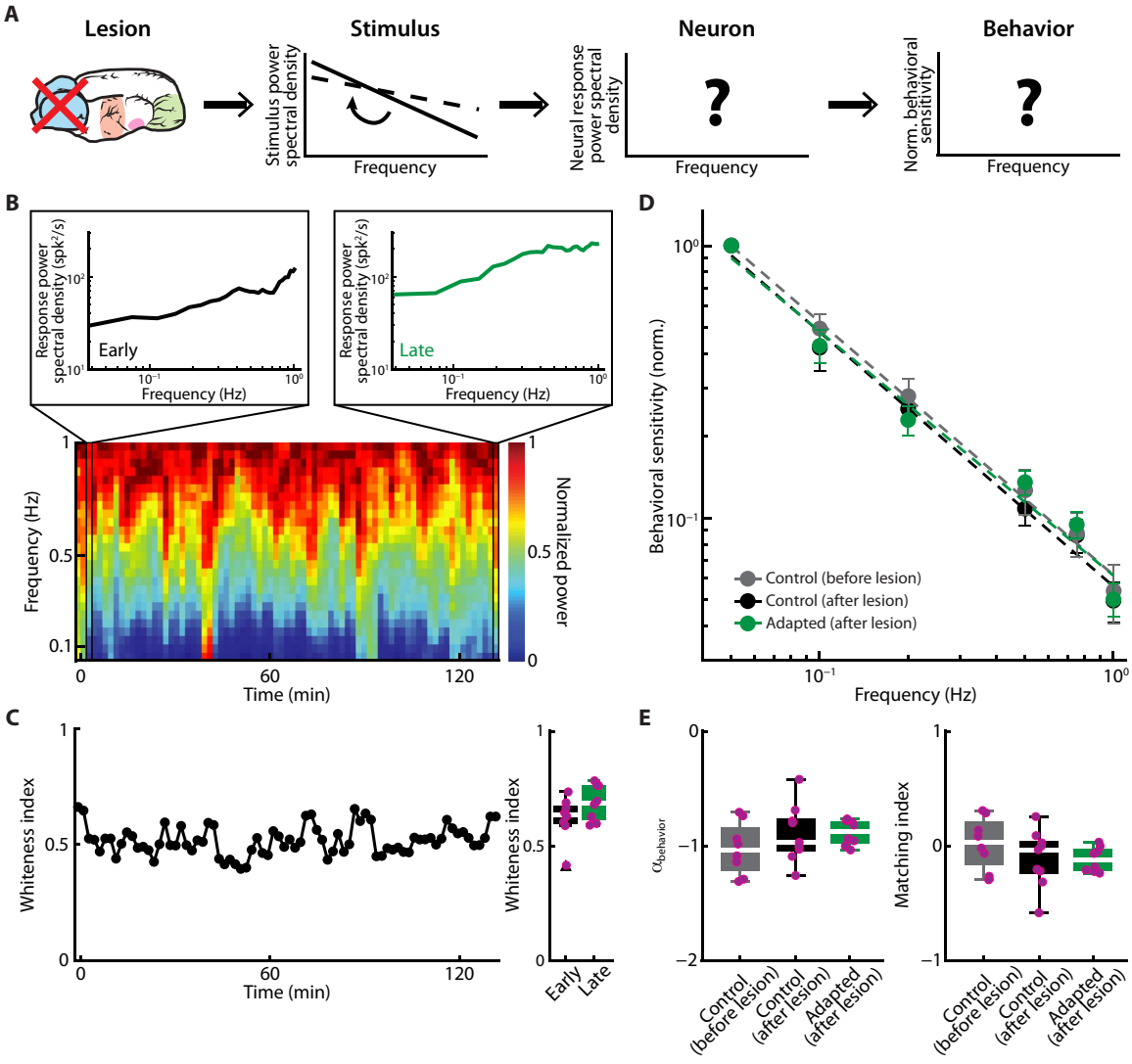

Fig. 5. Sensory adaptation requires descending input from the forebrain. (**A**) Schematic showing the brain (left); we lesioned the forebrain (left: red cross) before presenting the adaptation stimulus characterized by a power law exponent of −2 (middle left, solid black). Also shown is the power spectral density of the natural stimulus (middle left, dashed black). We investigated whether neural response power spectral density (middle right) as well as behavioral sensitivity (right) changed throughout stimulus presentation. (**B**) Spectrogram (i.e., running time power spectral density) of the response of an example PCell to the adaptation stimulus after lesion. The upper left and right insets show the response power spectral densities as a function of frequency for this cell early (left) and late (right) during stimulus presentation. (**C**) Left: Whiteness index as a function of time for this same PCell. Right: Population-averaged whiteness index values early (black) and late (green) during stimulus presentation. (**D**) Population-averaged behavioral sensitivity as a function of frequency before lesion (gray), as well as before (black) and after (green) stimulus presentation after lesion. (**E**) Left: Population-averaged behavioral exponents under control before lesion (gray), control after lesion (black), and after presenting the adaptation stimulus (green). Right: Population-averaged matching index values under control before lesion (gray), control after lesion (black), and after presenting the adaptation stimulus (green).

different conditions. Here, we have shown that the statistics of the sensory input experienced by weakly electric fish strongly depend on their longitudinal velocities when in the dark. Intuitively, when the animals move more, it is expected that the resulting stimuli will contain more high-frequency components and, thus, that the power spectral density will decay with an exponent lower in magnitude. In contrast, when the animals move less, it is expected that the resulting stimuli will contain more low-frequency components and, thus, that the power spectral density will decay with an exponent higher in magnitude. Thus, although they were obtained in the absence of light, our results suggest that weakly electric fish will experience stimuli with different power law exponents over the 24-hour day-night cycle. Specifically, because weakly electric fish are nocturnal (*18*), it is expected that they will move at higher velocities on average during the night than during the day and will, thus, experience sensory input characterized by different power law exponents under both conditions. Further studies are needed to test these hypotheses.

What are the functional roles of neural and behavioral adaptation? Our results show that, in response to adaptation stimuli, both neural and behavioral responses adapt. Specifically, while neural response power spectral densities became more independent of frequency, behavioral sensitivity was altered such that its power law exponent was

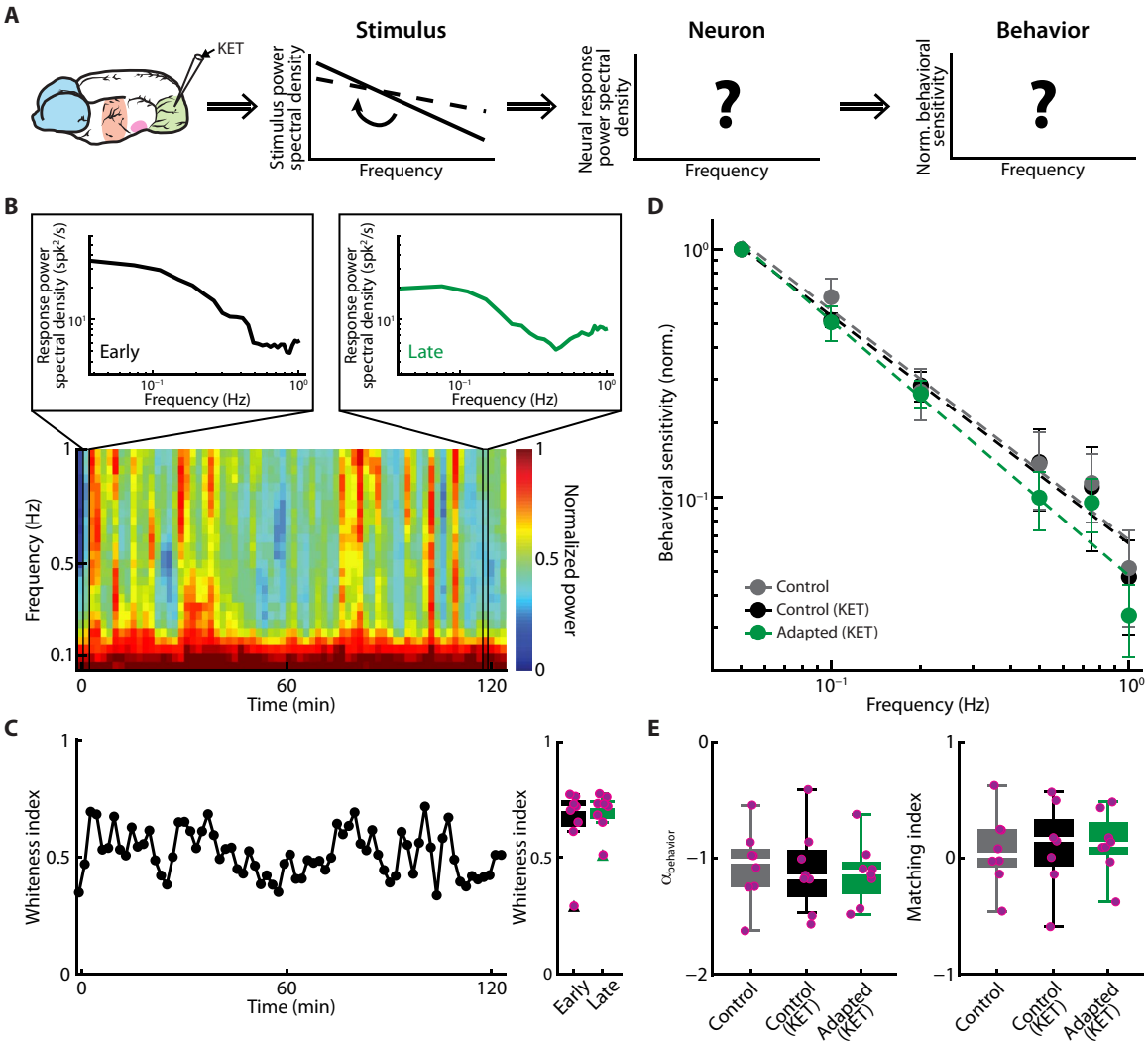

Fig. 6. Sensory adaptation requires descending serotonergic input from the raphe nuclei. (**A**) Schematic showing the brain (left); we injected the serotonergic antagonist KET into the ELL (pipette) before presenting the adaptation stimulus characterized by a power law exponent of −2 (middle, solid black). Also shown is the power spectral density of the natural stimulus (middle left, dashed black). We investigated whether neural response power spectral density (middle right) as well as behavioral sensitivity (right) changed throughout stimulus presentation. (**B**) Spectrogram (i.e., running time power spectral density) of the response of an example PCell to the adaptation stimulus after KET injection. The upper left and right insets show the response power spectral densities as a function of frequency for this cell early (left) and late (right) during stimulus presentation. (**C**) Left: Whiteness index as a function of time for this same PCell. Right: Population-averaged whiteness index values early (black) and late (green) during stimulus presentation. (**D**) Population-averaged behavioral sensitivity as a function of frequency before lesion (gray), as well as before (black) and after (green) stimulus presentation after KET injection. (**E**) Left: Population-averaged behavioral exponents under control before KET injection (gray), control after KET injection (black), and after KET injection after presenting the adaptation stimulus (green). Right: Population-averaged matching index values under control before KET injection (gray), control after KET injection (black), and after KET injection after presenting the adaptation stimulus (green).

closer to that of the adapting stimulus. It should be noted that, while the whiteness index values increased throughout adaptation, they did not reach unity. This could be for multiple reasons including limited recording time, as well as the possibility that responses are optimized for a linear-nonlinear system, rather than a linear one (*4*). Previous studies have found that, as a function of increasing frequency, both behavioral sensitivity and natural stimulus power spectral densities decayed with the same power law exponents (i.e., were "matched") (*10*). This makes intuitive sense as sensitivity is then highest for frequencies that are most highly represented in the stimulus, which would allow an animal to more strongly modulate its EOD frequency and, thus, appear stronger to potentially ward off an intruder (*10*). Our results provide further evidence supporting the hypothesis that the functional role of sensory adaptation is to maximize information transmission by sensory neurons through temporal whitening and to match behavioral sensitivity to stimulus statistics. We also note that the adaptation stimuli used in this study are unlikely to be encountered in the natural environment. This is because (i) their exponents were well outside of the observed range and (ii) their overall variance (i.e., area under the power spectral density curve) was the same, which is unlike that seen under seminaturalistic conditions. In the case of (i), we note that this is not a problem as the adaptation stimuli were used to attempt to elicit the maximum changes in ELL neural and behavioral responses. This fact could explain why adaptation did not lead to a perfect match between

behavioral sensitivity and the adapting stimulus' statistics. Rather, the observed power law exponents of the adapted behavioral sensitivity were at the lower and upper limits of the range observed under natural conditions, suggesting that this is the maximum operating range of the system, which matches to the range natural stimulus statistics. In the case of (ii), this implies that the overall intensity of the adaptation stimulus characterized by a power law exponent of zero should be increased relative to that of an adaptation stimulus characterized by a power law exponent of −2 to better match our observations under a more realistic setting. This increased intensity is not expected to qualitatively affect our results and should, in fact, give rise to stronger adaptation in neural responses than those observed in the current study. Further studies are however needed to test these predictions.

Mechanisms mediating sensory and behavioral adaption

Our results have shown that lesioning the forebrain did not affect neural or behavioral responses but did prevent adaptation. Hence, sensory and behavioral adaptation are likely caused by signals descending from the forebrain. Recent studies have uncovered the detailed anatomy of the forebrain of *Apteronotus leptorhynchus* with regard to learning and memory (*19*). In particular, they have identified reciprocal connections whose anatomy supports functions such as the computation of an error signal, which would be necessary to elicit sensory adaptation. One possibility is that descending signals from the forebrain are relayed via the midbrain TS, which then projects to the ELL via the nucleus praeeminentialis. Previous studies have revealed a variety of functions for descending input onto ELL PCells including gain control (*20*), adaptive cancellation of redundant sensory input (*21*, *22*), as well as generating neural responses to sensory input (*23*, *24*). Pharmacological inactivation of descending input strongly affects ELL PCell tuning to envelope stimuli (*13*). Further studies are needed to understand the nature of the computations being performed by the forebrain to determine sensory and behavioral adaptation to stimuli with different statistics.

Our results have further shown that the serotonergic antagonist KET also prevented sensory and behavioral adaptation. Previous studies have shown that ELL PCells receive large amounts of serotonergic input from the raphe nuclei (*25*). Activation of this input (e.g., by raphe nuclei stimulation) increases ELL PCell excitability via inhibition of small conductance calcium-activated potassium channels (*26*), which increases responsiveness to stimulation [see (*11*) for review]. Further studies have shown that increased excitability is likely mediated by 5-HT2 receptors (*27*). Our results reveal a previously unknown role for serotonergic input onto ELL PCells in that such input is necessary for adaptation. Thus, another possibility is that descending input from the forebrain is being relayed via serotonergic pathways. This possibility is, however, unlikely because neuromodulatory inputs typically do not transmit detailed information about the nature of sensory input (*28*). Rather, it is likely that serotonergic input is needed to elicit plasticity for descending synaptic input, as observed in other systems (*29*, *30*), and that the descending input from the forebrain is needed to determine the nature of changes in ELL PCell response properties such as to optimally encode stimuli with different statistics. Further studies are needed to characterize the response properties of neurons within the raphe nucleus to the adaptation stimuli used here.

Implications for other systems

It is very likely that our results will be applicable to other systems. First, there are multiple anatomical and physiological similarities between the electrosensory system of weakly electric fish and mammalian sensory systems (*31*). In particular, recent studies have found remarkable similarities between the electrosensory system of weakly electric fish and the vestibular system of nonhuman primates (*32*), which is not surprising from an evolutionary perspective as both are eighth nerve systems that have likely evolved from the lateral line (*33*, *34*). Moreover, a recent study in the vestibular system has shown that sensory neurons are adapted to the statistics of natural self-motion stimuli (*17*). In particular, central vestibular neurons optimally encode natural self-motion stimuli via temporal whitening, which is due to a match between their tuning and variability as well as the stimulus statistics (*17*). Given that temporal whitening has been observed in a wide range of sensory systems (*1*–*4*, *15*) and that sensory adaptation has been observed ubiquitously [see (*5*) for review], our results will likely be applicable to other systems. It was shown that visual cortical neurons could adapt their properties to optimally encode visual stimuli with different spectral frequency content (*4*), and it was proposed that the function of adaptation is to maximize information transmission of stimuli with time-varying statistics (*5*).

MATERIALS AND METHODS

Animals

The weakly electric fish *A. leptorhynchus* was used exclusively in this study. Animals of either sex were purchased from tropical fish suppliers and were acclimated to laboratory conditions according to published guidelines (*35*). All procedures were approved by McGill University's animal care committee and were performed in accordance with the guidelines of the Canadian Council on Animal Care.

Surgery

Surgical procedures have been described in detail previously (*13*, *24*). Briefly, 0.1 ± 0.5 mg of tubocurarine (Sigma-Aldrich) was injected intramuscularly to immobilize the fish for electrophysiology and behavioral adaptation experiments. The fish was then transferred to an experimental tank (30 cm by 30 cm by 10 cm) containing water from the animal's home tank and respired by a constant flow of oxygenated water through their mouth at a flow rate of ~10 ml/min. Subsequently, the animal's head was locally anesthetized with lidocaine ointment (5%; AstraZeneca, Mississauga, ON, Canada), the skull was partly exposed, and a small window was opened over the ELL recording site. For forebrain lesion experiments (electrophysiology: $n = 8$ PCells; average recording time, 112.4 ± 4 min; behavior: $n = 9$ fish; average recording time, 186.7 ± 35.3 min), the skull over both forebrain hemispheres was exposed and removed before lesioning the forebrain.

Stimulation

The EOD of *A. leptorhynchus* is neurogenic and therefore is not affected by injection of curare. All stimuli consisting of AMs of the animal's own EOD were produced by triggering a function generator to emit one cycle of a sine wave for each zero crossing of the EOD, as done previously (*36*). The frequency of the emitted sine wave was set slightly higher (~40 Hz) than that of the animal's own EOD, which allowed the output of the function generator to be synchronized to the animal's discharge. The emitted sine wave was subsequently multiplied with the desired AM waveform (MT3 Multiplier; Tucker Davis Technologies), and the resulting signal was isolated from the ground (A395 Linear Stimulus Isolator; World Precision Instruments). The isolated signal was then delivered through a pair of chloridized silver wire electrodes placed 15 cm away from the animal on either side of the recording tank perpendicular to the fish's rostrocaudal axis. The resulting signal measured

at the fish's skin was approximated using a dipole (1-mm distance between the two poles) positioned next to the fish 2 mm away.

We used stimuli consisting of a 5- to 15-Hz noise (fourth-order Butterworth) carrier waveform (i.e., AM) whose amplitude (i.e., envelope) was further modulated sinusoidally at frequencies ranging from 0.05 to 1 Hz. This constitutes a behaviorally relevant range of frequencies, which mimicked the envelope signals due to relative movement between two fish (*10*). Adaptation stimuli that consisted of a 100-s-long 5- to 15-Hz noise (fourth-order Butterworth) carrier signal whose amplitude was also noisy were played repetitively. The noisy amplitude was characterized by power spectra that decayed with exponents as a function of temporal frequency of either −2 (neurons: $n = 16$ PCells; average recording time, 106.3 ± 4.5 min; behavior: $n = 20$ fish; average recording time, 312 ± 26.7 min) or 0 (neurons: $n = 15$ PCells; average recording time, 108.7 ± 5.4 min; behavior: $n = 15$ fish; average recording time, 232 ± 29.8 min). We note that sensitivity and whiteness index values were already significant when only eight randomly selected neurons or fish were taken into account ($\alpha_{stim} = 0$: $\alpha_{neuron\ control} = 0.22 \pm 0.08$, $\alpha_{neuron\ adapted} = 0.5 \pm 0.07$, $P = 3.1 \times 10^{-2}$, whiteness index (WI): $P = 7.9 \times 10^{-3}$, $\alpha_{behavior\ control} = -0.83 \pm 0.05$, $\alpha_{behavior\ adapted} = -0.46 \pm 0.11$, $P = 7.8 \times 10^{-3}$; $\alpha_{stim} = -2$: $\alpha_{neuron\ control} = 0.54 \pm 0.12$, $\alpha_{neuron\ adapted} = 0.3 \pm 0.1$, $P = 7.8 \times 10^{-3}$, WI: $P = 1.6 \times 10^{-2}$, $\alpha_{behavior\ control} = -0.85 \pm 0.05$, $\alpha_{behavior\ adapted} = -1.25 \pm 0.15$, $P = 1.6 \times 10^{-2}$; Wilcoxon signed rank tests). The depth of modulation for both stimulus classes used during experimental stimulation was approximately 20% of the baseline EOD amplitude as in previous studies (*13*, *24*, *37*) as measured using a small dipole placed close to the animal's skin in the middle of the animal's rostrocaudal and dorsoventral axes (typically 0.2 mV cm^{-1}).

Pharmacology

The composition of the vehicle saline was as follows (all chemicals were obtained from Sigma): 111 mM NaCl, 2 mM KCl, 2 mM $CaCl_2$, 1 mM $MgSO_4$, 1 mM $NaHCO_3$, and 0.5 Mm NaH_2PO_4. The pH of the saline solution was 6.8. Glutamate (Sigma) and the 5-HT2 receptor antagonist KET (Sigma) were dissolved in saline before application, as done previously (*27*). Drug application electrodes were made using two-barrel KG-33 glass micropipettes [outer diameter (OD), 1.5 mm; internal diameter (ID), 0.86 mm; A-M Systems] and pulled by a vertical micropipette puller (Stoelting) to a fine tip that was subsequently broken to attain a tip diameter of approximately 5 μm for each barrel. The two barrels were used for separate application of either KET (100 mM) or NBOH (100 μM), as well as glutamate (1 mM). During ELL recordings for which we injected KET, we first used excitatory responses to glutamate application to confirm that we were within proximity of the pyramidal neuron we were recording from, as done previously (*24*, *38*). KET ($n = 8$ PCells; average recording time, 121.8 ± 1.1 min) was then ejected to the neuron to ensure a local effect. For behavioral recordings, injections of KET ($n = 8$ fish; average recording time, 240 ± 22.7 min) were performed bilaterally in ELL, as done previously (*12*, *13*, *24*). All pharmacological injections were performed using a duration of 130 ms at ~20 psi using a Picospritzer (General Valve) as done previously (*23*). For pharmacological experiments using KET, injections were done every 10 min during the adaptation period. We note that injecting saline alone as a control did not alter behavioral or neuronal activity as shown in previous studies (*24*, *39*).

Electrophysiology

We used well-established techniques to record extracellularly with Woods metal electrodes from PCells ($N = 59$ total; average baseline FR, 17.81 ± 1.23 Hz) (*40*) located within the lateral segment of the ELL based on recording depth and mediolateral placement of the electrode on the brain surface as done previously (*24*, *41*). All recordings were digitized at 10-kHz sampling rate using CED 1401plus hardware and Spike2 software (Cambridge Electronic Design) and stored on a computer hard disk for offline analysis.

Behavior

Animals were immobilized by an intramuscular injection of 0.1 to 0.5 mg of tubocurarine and set up in the recording tank similarly to the method described above. We note that behavioral responses were similar in both restrained and immobilized animals (*10*, *35*, *42*). Depending on the experimental protocol (pharmacology or lesion experiments), different surgeries were performed. For forebrain lesion experiments, both hemispheres of Tel were exposed, and the connection between the midbrain and forebrain was disrupted ($n = 9$ fish) to prevent any connectivity. For pharmacological manipulations, both ELLs were exposed on either side of the head to bilaterally inject KET ($n = 8$ fish; average recording time, 240 ± 22.7 min). Pipettes containing KET were placed approximately 200 to 300 μm below the surface of the hindbrain in the region of the apical dendrites of the PCells. Multiple injections (typically three to five) were performed to ensure that both hemispheres of ELL were sufficiently affected by the pharmacological agents. Stimuli were then presented as described above in the section on Stimulation to elicit behavioral responses before and after drug application or forebrain ablation. The animal's behavior was recorded through a pair of electrodes located at the rostrum and tail of the animal. The zero crossings of the recorded EOD signal were used to generate a binary sequence as described above that was low pass filtered (second-order Butterworth with 0.05-Hz cutoff) to obtain the time-varying EOD frequency.

Stimulus statistics

To calculate the frequency content of movement envelopes resulting from different velocities, we took 90-min recordings in different pairs of fish ($N = 4$), as done previously (*10*). Briefly, trials were performed in an experimental tank (45 cm by 35 cm by 15 cm) in the absence of light. One of the two fish was placed in a tube, while the other fish was freely moving around (fig. S1A). The tube was made of electrical transparent clay with small holes at the top and bottom to guarantee freshwater circulation. The clay was used to minimize mechanosensory or visual perception of the other fish outside the chirp chamber. A 2-mm transverse dipole adjacent to midpoint of the tube was used to measure the local electric field. The dipole signal was used to extract the envelope and was digitized at 50-kHz sampling rate using CED 1401plus hardware and Spike2 software (Cambridge Electronic Design, Cambridge, UK) and stored on a computer hard disk for offline analysis. Trials were videotaped from above using a camera (frame rate,8 fps; model UV-5803, Unique Vision, Longhua Town, Shenzhen, China) equipped with infrared illumination to extract the position of the freely moving fish relative to the dipole (Tracker software: https://physlets.org/tracker/). We first extracted the envelope from the stimulus as described previously (*43*) and computed the longitudinal velocity from the freely moving fish using its trajectories. To separate high from low velocities, we used the median longitudinal velocity in each recording (population average, 2.28 ± 0.15 cm/s) as a threshold of the measured longitudinal velocity of the freely moving fish. To obtain a continuous signal, we concatenated the envelope traces corresponding to the different activity levels accordingly. We note that concatenation will introduce discontinuities in the signal, which will increase power at high

frequencies but will have minimal effect on the low (i.e., <1 Hz) frequencies considered here. On average, the lengths of the traces obtained for low and high velocities did not differ significantly (Fig. 4B, inset; $P = 0.07$, Kolmogorov-Smirnov test). Furthermore, we generated a surrogate dataset where the signal was randomly segregated into segments of lengths drawn from the same distribution as obtained experimentally (see Fig. 4B, inset) and found similar power spectral densities (fig. S7A). Note that low and high movement envelopes could be significantly separated using a wide range of thresholds ranging from 50 to 150% of the median velocity (fig. S7B).

Data quantification

All data analyses were performed offline using custom-written codes in MATLAB software (MathWorks). Spike times were defined as the times at which the recorded neural signal crossed a given threshold value from below. A binary sequence was constructed from the spike times by discretizing time into bins of 0.1-ms width and setting the content of a given bin to 10,000 if a spike occurred within it or 0 otherwise. The time-varying FR was obtained by low pass filtering the binary sequence using a second-order Butterworth filter with cutoff frequencies 0.2, 0.35, 0.75, 1.5, 2.5, and 3.5 Hz for envelope frequencies 0.05, 0.1, 0.2, 0.5, 0.75, and 1 Hz, respectively, as done previously (*39*). Neural sensitivity for a given sinusoidal frequency was then measured as the ratio between the amplitude of the sinusoidal envelope stimulus as extracted by the dipole and the amplitude of the neural FR modulation. We also quantified neural sensitivity to the adaptation stimulus using linear systems identification techniques

$$G(f) = \frac{|P_{rs}(f)|}{P_{ss}(f)} \quad (1)$$

where $P_{rs}(f)$ is the cross-spectral density between the adaptation stimulus and the binary sequence, and $P_{ss}(f)$ is the adaptation stimulus power spectral density as a function of frequency f. The cross-spectral density was computed in MATLAB using nfft = 1024 × 260, noverlap = nfft/2 with multitaper techniques with eight Slepian tapers using the functions "cpsd" and "pwelch" in MATLAB, respectively. Behavioral responses were measured as changes in the animal's EOD frequency as done previously (*12*, *13*, *39*, *42*). Specifically, the sequence of inverse intervals between consecutive EOD zero crossings was used to compute the instantaneous EOD frequency, which was then interpolated to match the sampling rate of the envelope stimulus and further low pass filtered (second-order Butterworth filter with 0.05-Hz cutoff frequency). Behavioral sensitivity for a given sinusoidal frequency was then measured as the ratio between the amplitude of the sinusoidal envelope stimulus as extracted by the dipole and the amplitude of the sinusoidal EOD frequency modulation. The exponents were obtained by fitting a power law to the behavioral and neural sensitivities as a function of frequency, respectively. The whiteness index was measured by taking the normalized area under the power spectral density curve using a trapezoidal method and dividing by the maximum normalized area to achieve a value between 0 and 1 as done previously (*12*, *39*). The matching index between the behavioral sensitivity and the adapting stimulus was computed using $1 - |\alpha_{stim} - \alpha_{behavior}|$ as done previously (*12*), where α_{stim} and $\alpha_{behavior}$ are the best-fit power law exponents of the adapting stimulus (i.e., either −2 or 0) and of the behavioral sensitivity, respectively. We note that, as not all neurons could be held during the full 2-hour-long adaptation stimulus presentation, we always compared the average whiteness index values between the first and last three repetitions of the adaptation stimulus. Spectrograms were computed by estimating the power spectral density of the spiking response for every 100 s during stimulation using multitaper techniques with eight Slepian functions. Power spectra were then stacked for visualization. The time-dependent whiteness index was computed as described above for every 100 s during stimulation.

Theory posits that the response power spectral density $P_{rr}(f)$ is related to the gain $|G(f)|$, the stimulus power spectral density $P_{ss}(f)$, and the power spectral density of the trial-to-trial variability in the neural response $P_0(f)$ by the following equation (*17*, *44*)

$$P_{rr}(f) \approx P_0(f) + |G(f)|^2 P_{ss}(f) \quad (2)$$

Hence, we considered both the contributions of the variability as well as the tuning function $|G(f)|$ to predict the neural response to stimulation. Trial-to-trial variability was estimated from responses to at least three repeated presentations of the adaptation stimulus each lasting 100 s (*17*).

Neural response statistics

We computed FR, CV, BF, and the ISI distribution for each neuron early and late in stimulation from responses to three repeated presentations of the adaptation stimulus each lasting 100 s. ISI sequences were computed as the time intervals between consecutive spikes, and probability distributions of ISIs as a function of logarithmic time were partitioned into 60 bins. The CV was computed as the SD-to-mean ratio of the ISI probability density. Furthermore, BF was computed as the fraction of ISIs that is less than 10 ms (*26*, *38*, *45*).

Statistics

Statistical significance was assessed through Wilcoxon signed rank test at the $P = 0.05$ level unless otherwise stated. Values are reported as box plots unless otherwise stated. Error bars indicate mean ± SEM. On each box, the central mark indicates the median, and the bottom and top edges of the box indicate the 25th and 75th percentiles, respectively. The whiskers extend to the most extreme data points not considered outliers, and the outliers are plotted individually using the "▲" symbol. For datasets with $n \leq 10$, the individual data points are also shown.

SUPPLEMENTARY MATERIALS

Supplementary material for this article is available at http://advances.sciencemag.org/cgi/content/full/5/10/eaax2211/DC1

Fig. S1. Measures of neuronal activity are not significantly altered during presentation of adaptation stimuli characterized by a power law exponent of −2.

Fig. S2. Measures of neuronal activity are not significantly altered during presentation of adaptation stimuli characterized by a power law exponent of 0.

Fig. S3. Adaptive optimized coding cannot be predicted from changes in neuronal tuning to sinusoidal stimuli alone.

Fig. S4. Adaptive optimized coding cannot be predicted from changes in neuronal tuning to adaptation stimuli alone.

Fig. S5. Adaptive optimized coding can be predicted from changes in both neuronal tuning and variability during adaptation stimulus presentation.

Fig. S6. Behavioral gains as a function of frequency.

Fig. S7. Best-fit power law exponents for stimulus statistics are largely independent of the threshold used to separate low and high velocities.

Fig. S8. Neuronal response statistics are not changing after lesioning forebrain.

Fig. S9. Neuronal response statistics are not altered by KET injection.

REFERENCES AND NOTES

1. E. P. Simoncelli, B. A. Olshausen, Natural image statistics and neural representation. *Annu. Rev. Neurosci.* **24**, 1193–1216 (2001).
2. C. Pozzorini, R. Naud, S. Mensi, W. Gerstner, Temporal whitening by power-law adaptation in neocortical neurons. *Nat. Neurosci.* **16**, 942–948 (2013).
3. X. Pitkow, M. Meister, Decorrelation and efficient coding by retinal ganglion cells. *Nat. Neurosci.* **15**, 628–635 (2012).
4. T. O. Sharpee, H. Sugihara, A. V. Kurgansky, S. P. Rebrik, M. P. Stryker, K. D. Miller, Adaptive filtering enhances information transmission in visual cortex. *Nature* **439**, 936–942 (2006).
5. T. O. Sharpee, A. J. Calhoun, S. H. Chalasani, Information theory of adaptation in neurons, behavior, and mood. *Curr. Opin. Neurobiol.* **25**, 47–53 (2014).
6. R. Krahe, L. Maler, Neural maps in the electrosensory system of weakly electric fish. *Curr. Opin. Neurobiol.* **24**, 13–21 (2014).
7. E. I. Knudsen, Spatial aspects of the electric fields generated by weakly electric fish. *J. Comp. Physiol.* **99**, 103–118 (1975).
8. J. Henninger, R. Krahe, F. Kirschbaum, J. Grewe, J. Benda, Statistics of natural communication signals observed in the wild identify important yet neglected stimulus regimes in weakly electric fish. *J. Neurosci.* **38**, 5456–5465 (2018).
9. H. Fotowat, R. R. Harrison, R. Krahe, Statistics of the electrosensory input in the freely swimming weakly electric fish Apteronotus leptorhynchus. *J. Neurosci.* **33**, 13758–13772 (2013).
10. M. G. Metzen, M. J. Chacron, Weakly electric fish display behavioral responses to envelopes naturally occurring during movement: Implications for neural processing. *J. Exp. Biol.* **217**, 1381–1391 (2014).
11. C. G. Huang, M. J. Chacron, SK channel subtypes enable parallel optimized coding of behaviorally relevant stimulus attributes: A review. *Channels* **11**, 281–304 (2017).
12. C. G. Huang, Z. D. Zhang, M. J. Chacron, Temporal decorrelation by SK channels enables efficient neural coding and perception of natural stimuli. *Nat. Commun.* **7**, 11353 (2016).
13. C. G. Huang, M. G. Metzen, M. J. Chacron, Feedback optimizes neural coding and perception of natural stimuli. *eLife* **7**, e38935 (2018).
14. Z. D. Zhang, M. J. Chacron, Adaptation to second order stimulus features by electrosensory neurons causes ambiguity. *Sci. Rep.* **6**, 28716 (2016).
15. Y. Dan, J. J. Atick, R. C. Reid, Efficient coding of natural scenes in the lateral geniculate nucleus: Experimental test of a computational theory. *J. Neurosci.* **16**, 3351–3362 (1996).
16. M. J. Chacron, L. Maler, J. Bastian, Electroreceptor neuron dynamics shape information transmission. *Nat. Neurosci.* **8**, 673–678 (2005).
17. D. E. Mitchell, A. Kwan, J. Carriot, M. J. Chacron, K. E. Cullen, Neuronal variability and tuning are balanced to optimize naturalistic self-motion coding in primate vestibular pathways. *eLife* **7**, e43019 (2018).
18. M. E. Nelson, Electric fish. *Curr. Biol.* **21**, R528–R529 (2011).
19. A. C. Giassi, E. Harvey-Girard, B. Valsamis, L. Maler, Organization of the gymnotiform fish pallium in relation to learning and memory: I. Cytoarchitectonics and cellular morphology. *J. Comp. Neurol.* **520**, 3314–3337 (2012).
20. J. Bastian, Gain control in the electrosensory system mediated by descending inputs to the electrosensory lateral line lobe. *J. Neurosci.* **6**, 553–562 (1986).
21. J. Bastian, M. J. Chacron, L. Maler, Plastic and nonplastic pyramidal cells perform unique roles in a network capable of adaptive redundancy reduction. *Neuron* **41**, 767–779 (2004).
22. K. Bol, G. Marsat, E. Harvey-Girard, A. Longtin, L. Maler, Frequency-tuned cerebellar channels and burst-induced LTD lead to the cancellation of redundant sensory inputs. *J. Neurosci.* **31**, 11028–11038 (2011).
23. S. E. Clarke, L. Maler, Feedback synthesizes neural codes for motion. *Curr. Biol.* **27**, 1356–1361 (2017).
24. M. G. Metzen, C. G. Huang, M. J. Chacron, Descending pathways generate perception of and neural responses to weak sensory input. *PLOS Biol.* **16**, e2005239 (2018).
25. S. A. Johnston, L. Maler, B. Tinner, The distribution of serotonin in the brain of *Apteronotus leptorhynchus*: An immunohistochemical study. *J. Chem. Neuroanat.* **3**, 429–465 (1990).
26. T. Deemyad, L. Maler, M. J. Chacron, Inhibition of SK and M channel-mediated currents by 5-HT enables parallel processing by bursts and isolated spikes. *J. Neurophysiol.* **105**, 1276–1294 (2011).
27. E. A. Larson, M. G. Metzen, M. J. Chacron, Serotonin modulates electrosensory processing and behavior via 5-HT2-like receptors. *Neuroscience* **271**, 108–118 (2014).
28. L. M. Hurley, D. M. Devilbiss, B. D. Waterhouse, A matter of focus: Monoaminergic modulation of stimulus coding in mammalian sensory networks. *Curr. Opin. Neurobiol.* **14**, 488–495 (2004).
29. C. Kraus, E. Castren, S. Kasper, R. Lanzenberger, Serotonin and neuroplasticity — Links between molecular, functional and structural pathophysiology in depression. *Neurosci. Biobehav. Rev.* **77**, 317–326 (2017).
30. S. Matias, E. Lottem, G. P. Dugué, Z. F. Mainen, Activity patterns of serotonin neurons underlying cognitive flexibility. *eLife* **6**, e20552 (2017).
31. S. E. Clarke, A. Longtin, L. Maler, Contrast coding in the electrosensory system: Parallels with visual computation. *Nat. Rev. Neurosci.* **16**, 733–744 (2015).
32. M. G. Metzen, M. Jamali, J. Carriot, O. Ávila-Åkerberg, K. E. Cullen, M. J. Chacron, Coding of envelopes by correlated but not single-neuron activity requires neural variability. *Proc. Natl. Acad. Sci. U.S.A.* **112**, 4791–4796 (2015).
33. J. A. Alvez-Gomes, The evolution of electroreception and bioelectrogenesis in teleost fish: A phylogenetic perspective. *J. Fish Biol.* **58**, 1489–1511 (2001).
34. B. Fritzsch, H. Straka, Evolution of vertebrate mechanosensory hair cells and inner ears: Toward identifying stimuli that select mutation driven altered morphologies. *J. Comp. Physiol. A Neuroethol. Sens. Neural Behav. Physiol.* **200**, 5–18 (2014).
35. E. M. Hitschfeld, S. A. Stamper, K. Vonderschen, E. S. Fortune, M. J. Chacron, Effects of restraint and immobilization on electrosensory behaviors of weakly electric fish. *ILAR J.* **50**, 361–372 (2009).
36. J. Bastian, M. J. Chacron, L. Maler, Receptive field organization determines pyramidal cell stimulus-encoding capability and spatial stimulus selectivity. *J. Neurosci.* **22**, 4577–4590 (2002).
37. V. Hofmann, M. J. Chacron, Differential receptive field organizations give rise to nearly identical neural correlations across three parallel sensory maps in weakly electric fish. *PLOS Comput. Biol.* **13**, e1005716 (2017).
38. T. Deemyad, M. G. Metzen, Y. Pan, M. J. Chacron, Serotonin selectively enhances perception and sensory neural responses to stimuli generated by same-sex conspecifics. *Proc. Natl. Acad. Sci. U.S.A.* **110**, 19609–19614 (2013).
39. C. G. Huang, M. J. Chacron, Optimized parallel coding of second-order stimulus features by heterogeneous neural populations. *J. Neurosci.* **36**, 9859–9872 (2016).
40. K. Frank, M. C. Becker, Microelectrodes for recording and stimulation, in *Physical Techniques in Biological Research*, W. L. Nastuk, Ed. (Academic, 1964), vol. 5, pp. 22–87.
41. R. Krahe, J. Bastian, M. J. Chacron, Temporal processing across multiple topographic maps in the electrosensory system. *J. Neurophysiol.* **100**, 852–867 (2008).
42. M. G. Metzen, M. J. Chacron, Neural heterogeneities determine response characteristics to second-, but not first-order stimulus features. *J. Neurosci.* **35**, 3124–3138 (2015).
43. P. McGillivray, K. Vonderschen, E. S. Fortune, M. J. Chacron, Parallel coding of first- and second-order stimulus attributes by midbrain electrosensory neurons. *J. Neurosci.* **32**, 5510–5524 (2012).
44. H. Risken, *The Fokker-Planck Equation* (Springer, Berlin, 1996).
45. N. Toporikova, M. J. Chacron, SK channels gate information processing *in vivo* by regulating an intrinsic bursting mechanism seen *in vitro*. *J. Neurophysiol.* **102**, 2273–2287 (2009).

Acknowledgments

Funding: This research was supported by the Fonds de recherche du Québec: Nature et technologies and the Canadian Institutes of Health Research (M.J.C.). **Author contributions:** M.G.M. and M.J.C. designed the study. C.G.H. and M.G.M. collected and analyzed the data. C.G.H., M.G.M., and M.J.C. contributed to the interpretation of the results. C.G.H., M.G.M., and M.J.C. wrote the first draft of the manuscript. **Competing interests:** The authors declare that they have no competing interests. **Data and materials availability:** All data needed to evaluate the conclusions in the paper are present in the paper and/or the Supplementary Materials. All data and codes are freely available from the figshare repository (https://figshare.com/s/6935bf82bfcfb9b715dd). Additional data related to this paper may be requested from the authors.

Submitted 4 March 2019
Accepted 17 September 2019
Published 30 October 2019
10.1126/sciadv.aax2211

Citation: C. G. Huang, M. G. Metzen, M. J. Chacron, Descending pathways mediate adaptive optimized coding of natural stimuli in weakly electric fish. *Sci. Adv.* **5**, eaax2211 (2019).

Science Advances

Descending pathways mediate adaptive optimized coding of natural stimuli in weakly electric fish

Chengjie G. Huang, Michael G. Metzen and Maurice J. Chacron

Sci Adv **5** (10), eaax2211.
DOI: 10.1126/sciadv.aax2211